energy&fuels

pubs.acs.org/EF Article

Selective Decarboxylation of Fatty Acids Catalyzed by Pd-Supported Hierarchical ZSM-5 Zeolite

Marta Arroyo, Laura Briones, Héctor Hernando, José M. Escola, and David P. Serrano*

Cite This: *Energy Fuels* 2021, 35, 17167−17181 Read Online

ACCESS | Metrics & More | Article Recommendations

ABSTRACT: Decarboxylation of fatty acids is an interesting route for the production of renewable long-chain hydrocarbons that could replace fossil resources in the formulation of diesel and jet range fuels. The results reported in the present work demonstrate that Pd supported on hierarchical ZSM-5 zeolite allows for the decarboxylation of different fatty acids (stearic, oleic, and palmitic acids) to proceed under mild operation conditions (T = 250 °C and P_{H_2} = 6 bar) with over 90% selectivity toward middle distillate hydrocarbons and conversions in the range of 60−85%. This outstanding performance has been attributed to a combination of high accessibility and tailored acidity in the zeolitic support that favors the metal dispersion and promotes the interaction between Pd and acid sites. The presence of a hydrogen atmosphere, under low-pressure conditions, is required for activating the Pd sites. It is also noteworthy that the catalyst could be reused after washing with *n*-dodecane, retaining 74% of its initial stearic acid conversion with just a minor variation in the yield of C_{17} hydrocarbons.

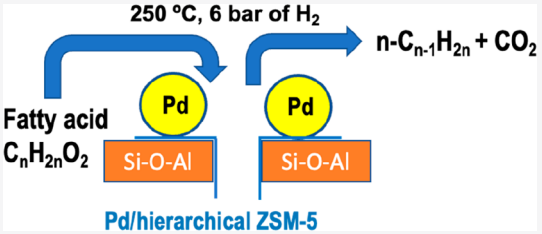

1. INTRODUCTION

The transformation of non-edible vegetable oils and free fatty acids into advanced biofuels is a subject of high interest because it provides products with properties very similar to those derived from fossil resources, thus facilitating their substitution by renewable fuels. Traditionally, vegetable oils have been converted into biodiesel [fatty acid methyl esters (FAMEs)] by means of transesterification with methanol using basic homogeneous catalysts (KOH and NaOH).[1,2] Although this technology is commercial and highly developed, enabling its usage even with waste cooking oils,[3,4] the thus-obtained biodiesel still shows a significant oxygen content, relatively high viscosity and cloud point, low volatility, and poor stability. Therefore, FAMEs are to be blended with conventional diesel in low shares to be used in diesel engines without requiring further modification.

Besides transesterification, a number of routes afford the production of hydrocarbon mixtures from vegetable oils or fatty acids, such as catalytic cracking, hydrodeoxygenation (HDO), and decarboxylation (DC).[5−12] Catalytic cracking of these feedstocks over different catalysts, mostly acid solids, has been extensively studied.[13−19] However, the fast catalyst deactivation by coke deposition and the high production of gases are important limitations of this route. Moreover, catalytic cracking usually leads to a great variety of products in terms of both hydrocarbon types and atom carbon number.

Mixtures of hydrocarbons with boiling points in the range of kerosene and diesel fuels can be obtained by means of HDO or DC of vegetable oils/triglycerides.[20−27] These products present the advantages of being formed mainly by long-chain paraffins, which provide them with superior properties in comparison to conventional diesel and jet fuels, because they show enhanced cetane indexes and lower emissions of particulate matter as a result of their reduced aromatic content.[28,29]

HDO of oleaginous feedstocks has been widely investigated using different metal-containing catalysts[30−35] and has reached the commercial stage. These are the cases of the processes developed by Neste to produce renewable diesel (NEXBTL technology)[36] and Eni in collaboration with Honeywell's UOP (ecofining process)[37] as well as Preem[38] and UPM[39] companies. However, HDO processes of vegetable oils require high pressures and significant hydrogen consumption,[40,41] which imply increased costs that may endanger their commercialization in the context of low petroleum prices.

A growing interest has appeared in recent years on DC as a promising and feasible alternative to attain advanced biofuels from vegetable oils and free fatty acids.[42−46] This route presents a number of advantages, because it affords the production of long-chain hydrocarbons, with a high share of the diesel fraction, operating under mild conditions, i.e., low

Special Issue: 2021 Pioneers in Energy Research: Javier Bilbao

Received: May 5, 2021
Revised: August 5, 2021
Published: August 16, 2021

https://doi.org/10.1021/acs.energyfuels.1c01373
Energy Fuels 2021, 35, 17167−17181

pressures and intermediate temperatures. Moreover, DC does not need a high hydrogen supply because this component is mainly required to activate the catalysts and avoid their deactivation.[47,48] DC of oleaginous feedstocks has been mostly investigated using both noble and transition metals deposited over different supports (although there is some case using unsupported metals[49]). The most common catalyst for DC of fatty acids is Pd/C, because metallic palladium is particularly suitable for promoting DC reactions.[50−52] However, the regeneration of Pd/C catalysts raises some concerns because calcination is precluded. Thus, novel catalysts with enhanced performance have been recently proposed for DC of different fatty and organic acids as well as vegetable oils based on the use of other supports, such as alumina, zirconia, mesoporous silica, nitrogen-doped mesoporous carbons, folded sheet material (FSM), ordered mesoporous silica, Al-SBA-15, and metal−organic frameworks (MOFs).[53−62]

Interestingly, despite the high relevance of zeolites as catalysts in the petrochemical industry and in a large variety of biomass transformations, these materials have just recently been investigated in the DC of fatty feedstocks. In this regard, Pt supported on zeolite 5A beads gave rise to high yields of heptadecane (>70%) in the conversion of oleic acid.[63] Likewise, Pt-SAPO-34 led to a high heptadecane selectivity in the conversion of oleic acid,[64] whereas K-based faujasite (FAU) showed activity in the DC/decarbonylation of methyl laurate.[65] On the other hand, Ni supported over mordenite zeolite promoted the deoxygenation of stearic acid, yielding 47% heptadecane.[66] Finally, Co supported on zeolite NaX showed high conversion (83.7%) in the DC of stearic acid, although with a relatively low heptadecane yield (28%).[67] In this way, an important issue to be addressed is the role played by the acid sites present in zeolites because they may reinforce the catalytic activity of the metal centers but, at the same time, could promote undesired secondary reactions.

In this context, the current work reports the remarkable catalytic properties of Pd supported over hierarchical ZSM-5 zeolites in the fatty acid DC. As far as we know, this catalytic system has not yet been investigated in the DC of fatty feedstocks. A proper combination of accessibility and acidity in this material is proposed here as the major reason for the high activity and selectivity toward DC products thus achieved. Moreover, the work discloses the effect of the most important reaction parameters and proves the feasibility of reusing the Pd/h-ZSM-5 catalyst.

2. EXPERIMENTAL SECTION

2.1. Catalyst Preparation. The hierarchical ZSM-5 zeolites were prepared according to the protozeolitic unit silanization method published elsewhere.[68] The reagents used were tetraethylorthosilicate (TEOS, 98%, Aldrich), tetrapropylammonium hydroxide (TPAOH, Alfa, 40%, v/v, aqueous solution), aluminum isopropoxide (AIP, Aldrich), phenylaminopropyltrimethoxysilane (PHAMPTMS, Aldrich), and distilled water. The composition of the raw mixture was as follows: $x Al_2O_3/60SiO_2/11TPAOH/1500H_2O$, where x was modified for achieving Si/Al molar ratios in the gel of 30, 100, and ∞, respectively. The organosilane (PHAMPTMS) was incorporated into the gel after a precrystallization step at 90 °C, with a proportion of 5 mol % regarding the TEOS content. Crystallization was achieved by hydrothermal treatment at 170 °C for 7 days. The Al-containing materials thus obtained were named as h-ZSM-5 (33) and h-ZSM-5 (122), wherein the number in parentheses represents their actual Si/Al molar ratio, determined by inductively coupled plasma atomic emission spectroscopy (ICP−AES) analyses. The sample with Si/Al = ∞ was named as h-silicalite-1. Palladium was added to the zeolitic supports by incipient wetness impregnation with an aqueous solution containing 1 wt % Pd ($PdCl_2$, 99.999%, Aldrich) under acidic pH (~2). After impregnation, the sample was sonicated for 30 min to favor the Pd species dispersion, and finally, it was evaporated under vacuum for 6 h to remove the solvent. The target Pd content in the final catalyst was 1 wt %.

Thereafter, the solid was dried in an oven at 110 °C for 12 h and calcined under static air at 550 °C for 5 h (heating ramp rate of 20 °C/min). The activation of the catalysts was carried out by reduction in a quartz reactor under a 30 mL/min hydrogen flow, heating to 450 °C with a ramp rate of 2 °C/min, with this temperature being held for 1 h. Subsequently, the activated catalyst was cooled to room temperature under a 20 mL/min nitrogen flow.

2.2. Catalyst Characterization. High-angle X-ray diffraction (XRD) patterns of the calcined samples were obtained in a Philips X'PERT MPD diffractometer using Cu Kα radiation in the interval of 5−75° using a step size of 0.1° and a counting time of 10 s. ICP−AES analyses were performed with a Varian VISTA-AX CCD spectrophotometer.

Argon adsorption−desorption isotherms at 87 K were obtained in a Quantachrome AUTOSORB device. Prior to the analyses, the samples were outgassed at 300 °C under vacuum for 3 h. The surface area was calculated by the Brunauer−Emmett−Teller (BET) method. The micropore surface areas and pore size distributions were attained by application of the non-local density functional theory (NLDFT) model, under the assumption of cylindrical pore geometry.

The acidic properties were determined by pyridine adsorption/desorption monitored by Fourier transform infrared (FTIR) spectroscopy. The samples were prepared as self-supporting wafers (⌀ = 13 mm, 8−15 mg/cm^2), mounted into a 316SS cell provided with CaF_2 windows. Wafers were dried overnight at 120 °C and activated at 500 °C for 2 h under vacuum prior to the adsorption of the probe molecule (pyridine) at 150 °C and a pressure of 4 mbar. All spectra were recorded with a resolution of 4 cm^{-1} in the 4000−1000 cm^{-1} range using a Jasco FT/IR-4600 equipped with a triglycine sulfate (TGS) detector (background, 64 scans; samples, 32 scans). The strength of the acid sites was studied by recording the FTIR spectra after treating the sample at different desorption temperatures (150, 250, 350, and 450 °C). The quantification of the acid sites was performed using the following bands (vibration mode of pyridine) and absorption coefficients: pyridinium PyH^+ band at 1545 cm^{-1} (ε = 1.67 cm mol^{-1}) and pyridine PyL band at 1455 cm^{-1} (ε = 2.2 cm mol^{-1}).[69]

Transmission electron microscopy (TEM) images were taken in a Philips TECNAI 20 microscope equipped with a LaB_6 filament under an accelerating voltage of 200 kV. Previously, the samples were dispersed in acetone using an ultrasonic bath, and subsequently, they were deposited over a carbon-coated copper grid.

2.3. Catalytic Tests of Fatty Acid DC. The catalytic experiments were carried out in a stainless-steel autoclave heated externally and equipped with a stirrer. In every reaction, the catalyst (0.4 g) was loaded along with 20 g of a 10 wt % single fatty acid solution in *n*-dodecane (≥99%, Sigma-Aldrich). The studied fatty acids were stearic acid (purity of >95%, Sigma-Aldrich), oleic acid (purity of >93%, Sigma-Aldrich), and palmitic acid (purity of >99%, Sigma-Aldrich). Then, the desired hydrogen pressure (3−25 bar) was fixed, and the reactor was heated to the specified temperature (225−300 °C), holding for a fixed time (180 min) under stirring. After the reaction finished, the reactor was cooled to 80 °C and then opened; thus, the gaseous and liquid products were separated in an ice-cooled condenser. Additionally, the liquid product was filtered under vacuum with a filtration plate at 110 °C to separate the catalyst and avoid the precipitation of any unreacted fatty acid as well.

A Varian CP-4900 Micro gas chromatograph (GC) was used for the analysis of the gaseous phase, which was equipped with Molsieve 5 Å PLOT and ParaPLOT U/Q columns and thermal conductivity detector (TCD). This setup enabled the detection and measurement of H_2, CO, CO_2, and hydrocarbons from C_1 to C_4. For the analysis of the liquid products, a Bruker SCIEN 456-GC, provided with a fused

https://doi.org/10.1021/acs.energyfuels.1c01373
Energy Fuels 2021, 35, 17167−17181

Table 1. Physicochemical Properties of the Catalysts

sample	Pd/h-ZSM-5 (33)	Pd/h-ZSM-5 (122)	Pd/h-silicalite
Si/Al molar ratio	33	122	∞
Pd content (wt %)	0.96	0.94	0.90
average Pd particle size (nm)	13	17	20
BET surface area ($m^2\ g^{-1}$)	477	486	491
micropore surface area (m^2/g)	209	265	294
external/mesopore surface area (m^2/g)	268	221	197

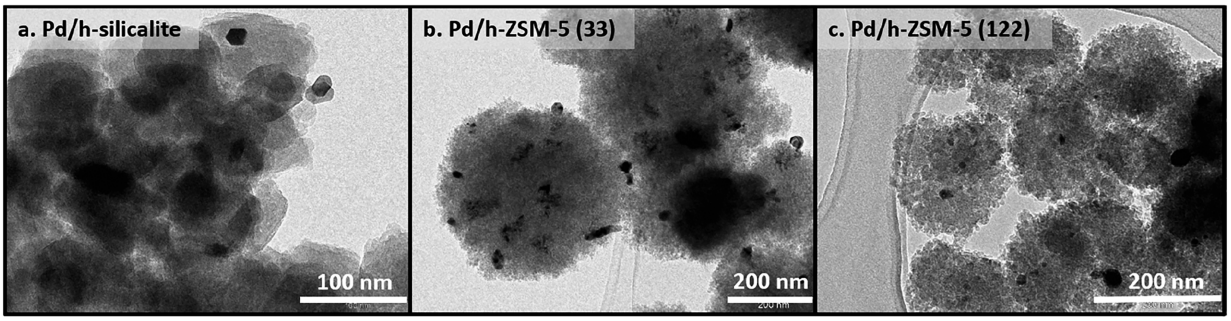

Figure 1. TEM images of the different catalysts.

silica BR 5 column (0.25 mm internal diameter and 30 m length) and flame ionization detector (FID), was used. This setup allowed for the separation and measurements of the C_4−C_{20} hydrocarbons. Additionally, a silylation procedure based on the EN-14105 standard was employed for a better analysis of the fatty acids.[60] The identification of the different *n*-alkanes has been carried out using a calibration mixture made up of all of the linear paraffins within the C_{10}−C_{18} range; therefore, the respective retention times allowed for their identification, and areas under the peak allowed for their quantification. The mass concentrations of the different hydrocarbons (g/L) were determined using an internal standard (1,2,3,4-tetrahydronaphthalene). Thereby, the following formula has been used for the calculations:

$$C_{\text{mass compound}} = \frac{\text{GC area}_{\text{compound}}}{\text{GC area}_{\text{internal standard}}} \times C_{\text{mass internal standard}}$$

For all of the calculations, a response factor of 1 was used. This assumption was checked and agrees well with the hydrocarbon nature of the obtained compounds.

The following selectivities were defined and calculated from the hydrocarbon product distribution:

(i) Selectivity by groups, gathering the different hydrocarbons into three fractions (C_1−C_4, C_5−C_{12}, and C_{13}−C_{18}) and determined as

$$\text{selectivity to } C_x\text{−}C_y = \frac{\sum \text{masses of the hydrocarbons between } C_x \text{ and } C_y}{\sum \text{masses of all produced hydrocarbons}} \times 100$$

wherein *x* and *y* stand for the starting and final carbon atom numbers, respectively, of each reaction fraction.

(ii) Selectivity toward C_{17} and C_{18} hydrocarbons:

$$C_{17}\text{ selectivity} = \frac{\sum \text{masses of } C_{17} \text{ hydrocarbons}}{\sum \text{masses of all produced hydrocarbons}} \times 100$$

$$C_{18}\text{ selectivity} = \frac{\sum \text{masses of } C_{18} \text{ hydrocarbons}}{\sum \text{masses of all produced hydrocarbons}} \times 100$$

(iii) Selectivity toward normal (linear) hydrocarbons:

$$n\text{-}(C_x\text{−}C_y)\text{ selectivity} = \frac{\sum \text{masses of } n\text{-hydrocarbons between } C_x \text{ and } C_y}{\sum \text{masses of all produced hydrocarbons}} \times 100$$

$$n\text{-}C_{17}\text{ selectivity} = \frac{\text{mass of } n\text{-}C_{17} \text{ hydrocarbons}}{\sum \text{masses of all produced hydrocarbons}} \times 100$$

$$n\text{-}C_{18}\text{ selectivity} = \frac{\text{mass of } n\text{-}C_{18} \text{ hydrocarbons}}{\sum \text{masses of all produced hydrocarbons}} \times 100$$

Finally, the relative extension of DC and HDO reactions was determined as follows:

$$\frac{\text{DC}}{\text{DC + HDO}} = \frac{\text{total mass of } C_{17} \text{ hydrocarbons}}{\text{total mass of } C_{17} \text{ and } C_{18} \text{ hydrocarbons}}$$

3. RESULTS AND DISCUSSION

3.1. Properties of the Catalysts. Two hierarchical ZSM-5 samples, possessing different Si/Al ratios, have been used as Pd supports. In addition, a pure silica hierarchical MFI zeolite (silicalite 1) was also prepared as a reference to better establish the effect of the support acidity. The three supports were impregnated with the same amount of Pd (1 wt %). Details

Table 2. Concentration of Brønsted and Lewis Acid Sites over h-ZSM-5 (33) and h-ZSM-5 (122) Supports Calculated from FTIR Spectra of Pyridine Adsorption Measurements[a]

	h-ZSM-5 (122)			h-ZSM-5 (33)		
T (°C)	C_B (mmol/g)	C_L (mmol/g)	C_B/C_L	C_B (mmol/g)	C_L (mmol/g)	C_B/C_L
150	0.052	0.053	0.98	0.168	0.104	1.61
250	0.045	0.046	0.98	0.154	0.066	2.33
350	0.034	0.015	2.37	0.118	0.036	3.27
450	0.026	0.007	3.71	0.076	0.024	3.16

[a] C_B, concentration of Brønsted acid sites; C_L, concentration of Lewis acid sites.

https://doi.org/10.1021/acs.energyfuels.1c01373
Energy Fuels 2021, 35, 17167−17181

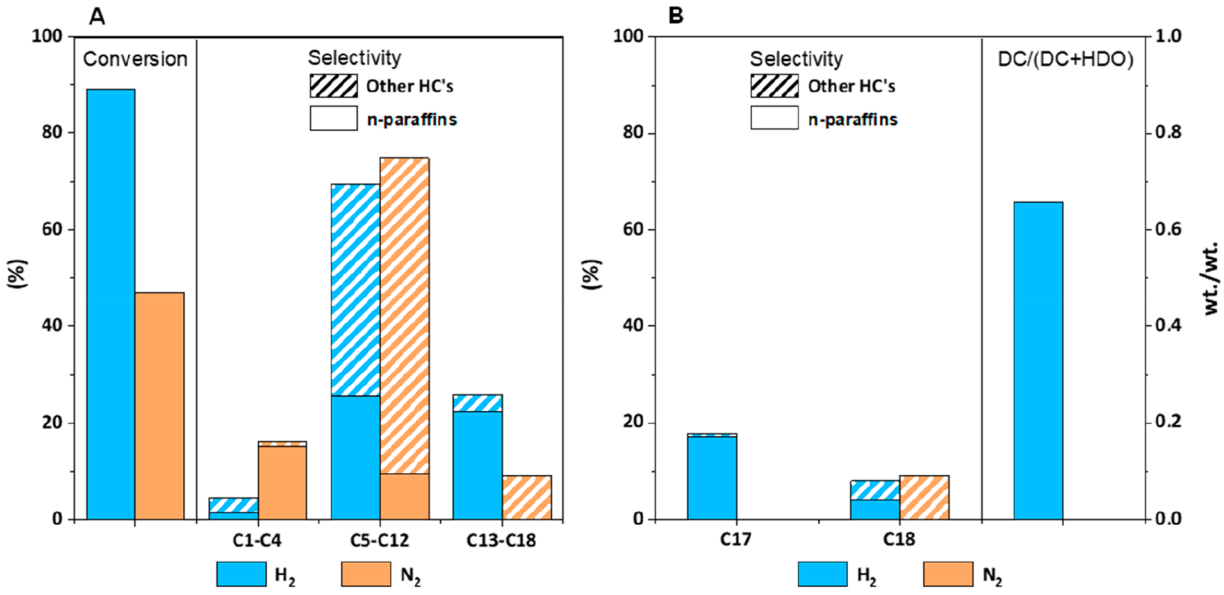

Figure 2. Influence of the reaction atmosphere in the transformation of stearic acid: (A) conversion and selectivity by hydrocarbon fractions along with the *n*-paraffin share and (B) selectivity toward C_{17} and C_{18} hydrocarbons and DC/(DC + HDO) ratio [T = 300 °C, t = 180 min, P = 6 bar of H_2 or N_2, and catalyst = Pd/h-ZSM-5 (122)].

about the properties of these materials can be found elsewhere,[70−72] as summarized in Table 1.

The three samples present BET surface areas above 470 m^2 g^{-1} that clearly surpasses the typical values for conventional micrometer size ZSM-5 zeolites (BET surface area of ∼375−400 m^2 g^{-1}).[73] Moreover, they exhibit a high contribution of mesopore/external surface, with values superior to 190 m^2 g^{-1} that tend to increase upon diminishing the Si/Al atomic ratio. These features are consistent with the presence of a hierarchical porosity as a consequence of the incorporation of the PHAPTMS organosilane into the synthesis gel that acts as mesopore generating agent. Therefore, the three Pd-containing zeolite samples show a great deal of fully accessible mesopore/external surface areas, although preserving a considerable share of the typical microporosity of the MFI structure.

The Si/Al atomic ratios of the ZSM-5 samples (33 and 122) were slightly higher than that of the of the final gel (Si/Al = 31.5 and 105, respectively), showing that, in general, both Si and Al are incorporated into the zeolite in a very similar extension. Likewise, the palladium content was slightly below the theoretical loading (1 wt %). Figure 1 illustrates TEM images of the three catalysts, wherein the Pd particles (black dots) may be distinguished over the 100−300 nm size globular particles of the hierarchical MFI supports. The average Pd crystal size was obtained by direct measurements of more than 100 Pd particles in the TEM images, showing that it increased with the Si/Al atomic ratio, from 13 nm [Pd/h-ZSM-5 (33)] to 20 nm (Pd/h-silicalite). This fact provides evidence of the occurrence of interactions between the Pd particles and the Al sites of the zeolitic support that aid to obtain a better metal dispersion.

The concentration of Brønsted and Lewis acid sites of the parent zeolites, calculated from FTIR spectra of pyridine adsorption measurements, is shown in Table 2. As expected, the concentration of both types of acid sites increases with the Al content of the supports. They pointed out a higher ratio of Brønsted/Lewis (C_B/C_L) for h-ZSM-5 (33) than for h-ZSM-5 (122) within the range of 150−350 °C and the opposite at 450 °C. Both samples present a relatively high concentration of Lewis acid sites compared to conventional ZSM-5 samples. This fact can be related to their hierarchical features that provide them a higher external/mesopore surface area, making Brønsted acid sites more prone to undergo dehydroxylation phenomena into Lewis sites during calcination. Additionally, for both zeolites, the Brønsted acid sites were stronger than the Lewis acid sites, because the C_B/C_L ratio augmented with the temperature.

3.2. Fatty Acid DC. Most of the catalytic tests in this work have been performed using stearic acid as the model substrate to identify the most convenient reaction conditions as well as the MFI zeolite support that exhibits the best performance, for promoting DC reactions with high selectivity toward long-chain hydrocarbons, in particular, toward heptadecane. Thereafter, the effect of the nature of the fatty acid was also investigated using oleic and palmitic acids as feedstocks. On the other hand, the catalysts used here are based on Pd supported over hierarchical ZSM-5, which, to the best of our knowledge, have not been assessed before for the DC of fatty acids. Moreover, as far as we know, this is the first time in which ZSM-5 zeolite is reported as a catalyst component for the DC of fatty acids proceeding with both high activity and selectivity. Previous works, showing that the occurrence of ZSM-5 in the makeup of several catalysts facilitated the formation first of C_{17} fragments from soybean oil and methyl oleate at 500 °C,[74−76] were really aimed to promote dehydrocyclization−cracking reactions instead of just fatty acid DC.

3.2.1. Influence of the Reaction Atmosphere. One crucial point in the DC of fatty acids is the effect of the reaction atmosphere because, in principle, this type of transformation could proceed in the absence of hydrogen. To establish the effect of the reaction atmosphere, the transformation of stearic acid was carried out at 300 °C under 6 bar of either nitrogen or hydrogen. Figure 2 illustrates the results thus obtained in terms of stearic acid conversion and selectivity toward the different

https://doi.org/10.1021/acs.energyfuels.1c01373
Energy Fuels 2021, 35, 17167−17181

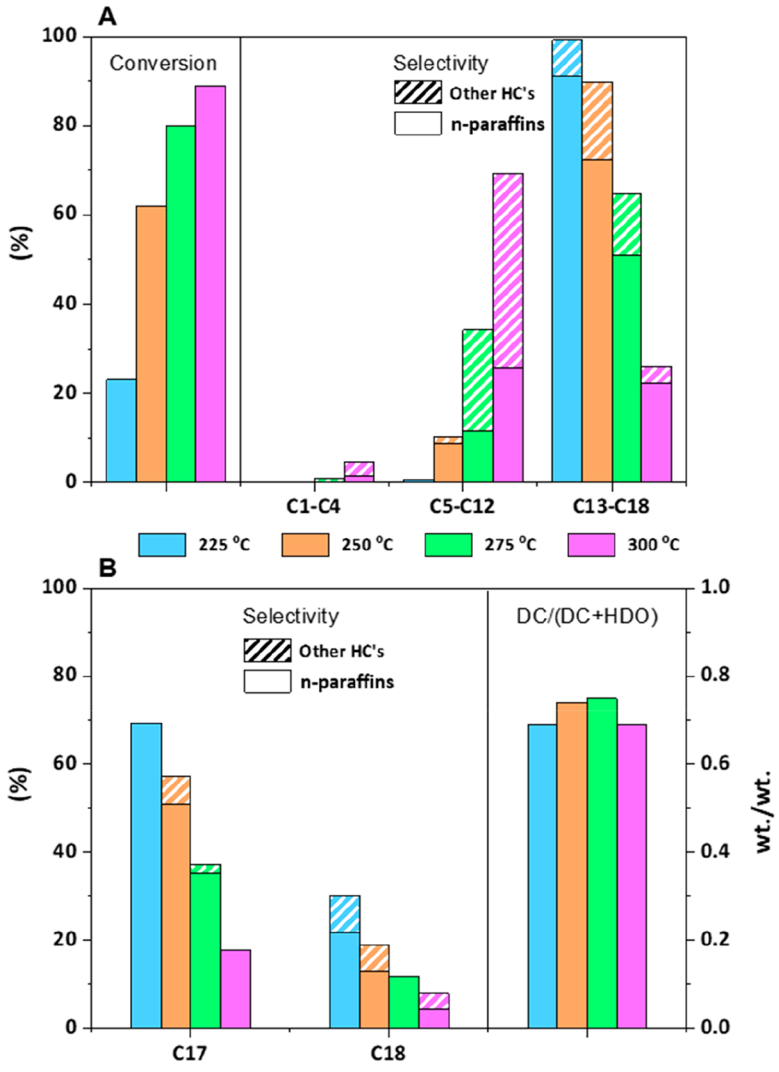

Figure 3. Influence of the reaction temperature: (A) conversion and selectivity by hydrocarbon fractions along with the *n*-paraffin share and (B) selectivity toward C_{17} and C_{18} hydrocarbons and DC/(DC + HDO) ratio [T = 225−300 °C, t = 180 min, P_{H_2} = 6 bar, catalyst = Pd/h-ZSM-5 (122)].

fractions and components of interest, also including the values of the DC/(DC + HDO) ratio.

It is noteworthy the meaningful increase in the stearic acid conversion that occurs when using hydrogen (89%) in comparison to the test performed with nitrogen (47%) can be assigned to a strong promotion effect of the Pd catalytic activity in the presence of H_2. With regard to the product distribution, a larger selectivity toward C_{13}−C_{18} hydrocarbons was attained (26 versus 9%) under a hydrogen atmosphere at the expense in the decrease of the selectivity toward gases (4.6 versus 16%) and gasolines (69.3 versus 74.8%). Moreover, the presence of hydrogen renders a higher content of *n*-paraffins within the C_5−C_{12} and C_{13}−C_{18} fractions in comparison to nitrogen. It must be said that, besides *n*-paraffins, the remaining products are branched hydrocarbons (mostly isoparaffins). Therefore, both the cracking and isomerization activities of the zeolite catalyst, originated by its acid sites, are attenuated when using the hydrogen atmosphere.

An important fact is that, under a nitrogen atmosphere, almost no C_{17} hydrocarbons were detected, suggesting the practical absence of pure DC reactions. Nevertheless, it could be assumed that some C_{17} hydrocarbons are really formed, being subsequently very quickly cracked into lighter components; hence, they are not observed among the reaction products. In contrast, in the presence of hydrogen, C_{17} hydrocarbons were obtained in significant amounts. In fact, the production of C_{17} was higher than that of C_{18} hydrocarbons for the test performed in a hydrogen atmosphere, resulting in a DC/(DC + HDO) ratio of 0.69.

These results denote the relevant role of the gas atmosphere on both catalytic activity and product distribution, showing the positive effect of the use of hydrogen on the DC pathway, although its presence is not really required according to the stoichiometry of the DC reaction. This finding is in line with an earlier study[77] about the DC of stearic acid over Pd supported onto WO_3/ZrO_2 that also observed an enhanced selectivity to *n*-alkanes when hydrogen gas was present instead of an inert gas. Consequently, the rest of the tests reported here were carried out using a hydrogen atmosphere.

3.2.2. Influence of the Reaction Temperature. Although the previous section pointed out that DC was favored under a hydrogen atmosphere, the selectivity toward heptadecane was

https://doi.org/10.1021/acs.energyfuels.1c01373
Energy Fuels 2021, 35, 17167−17181

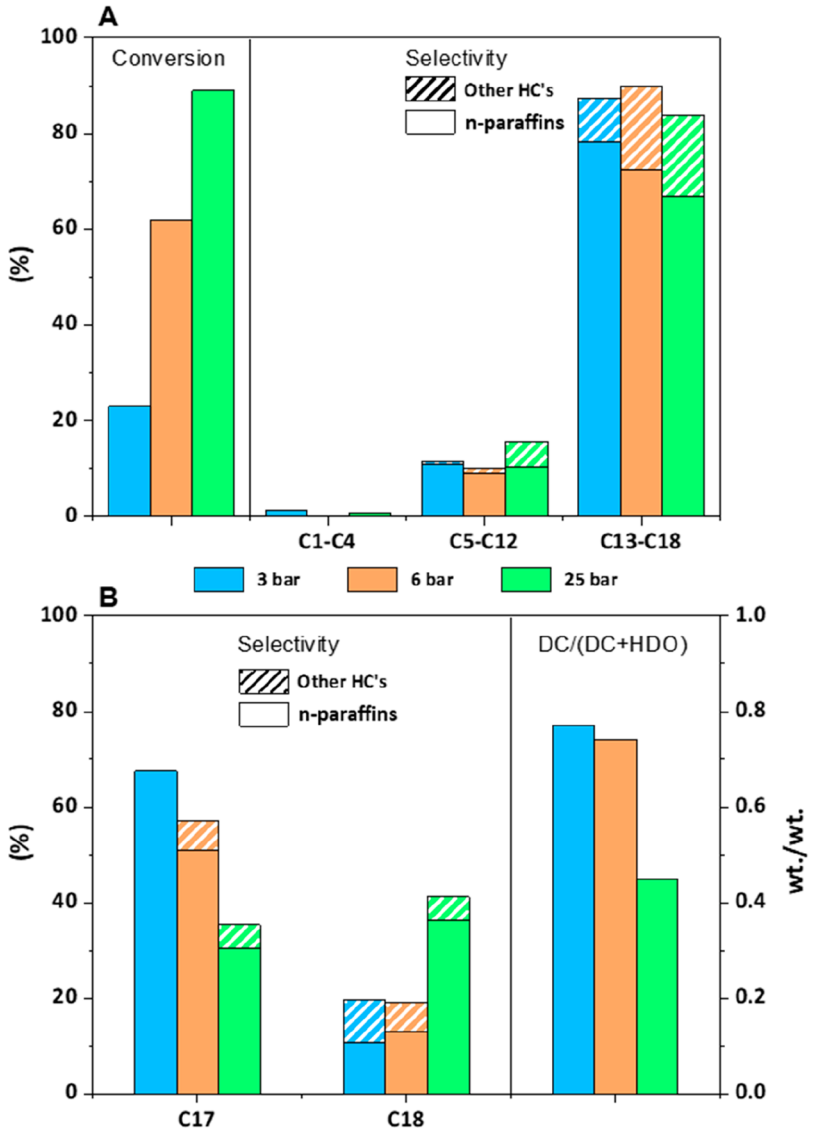

Figure 4. Influence of the H_2 pressure: (A) conversion and selectivity by hydrocarbon fractions along with the *n*-paraffin share and (B) selectivity toward C_{17} and C_{18} hydrocarbons and DC/(DC + HDO) ratio [T = 250 °C, t = 180 min, P_{H_2} = 3, 6, and 25 bar, and catalyst = Pd/h-ZSM-5 (122)].

still low (17.9%) as a result of cracking reactions occurring extensively. Because those tests were carried out at 300 °C, the influence of the reaction temperature was investigated in the range of 225−300 °C to ascertain whether working under milder conditions may enhance the selectivity toward DC and reduce the extent of cracking.

Figure 3A illustrates the conversion and selectivity by hydrocarbon fractions along with the share of *n*-paraffins attained at different temperatures. The abatement in temperature, although diminishing the conversion of stearic acid, induces a very positive effect on the product distribution because the formation of C_1−C_4 and C_5−C_{12} fractions is markedly reduced. Thus, almost no gaseous products are obtained when working below 300 °C, whereas the selectivity toward gasoline-range hydrocarbons is lower than 10% for temperatures of 225 and 250 °C. These results show that the occurrence of cracking reactions, catalyzed by the strong acid sites of the ZSM-5 zeolite, can be prevented by conveniently lowering the reaction temperature. As a consequence, the selectivity toward middle distillates (C_{13}−C_{18} fraction) is enhanced, hiking from 26% at 300 °C to almost 100% at 225 °C. In the same way, the production of both C_{17} and C_{18} hydrocarbons is favored when decreasing the reaction temperature as a result of a lower extent of the cracking reactions. Thus, as shown in Figure 3B, the selectivity toward C_{17} varies from 17.9% at 300 °C to 69.1% at 225 °C, having a high share of *n*-C_{17} (>90%). Likewise, the selectivity toward C_{18} hydrocarbons increased from 8.0% at 300 °C to 30.1% at 225 °C. Interestingly, the DC/(DC + HDO) ratio for all of these tests is in the range of 0.69−0.75, which is indicative of DC taking place in a higher extension than HDO. Additionally, this ratio scarcely varies with the temperature, suggesting that both deoxygenation pathways (DC and HDO) possess similar activation energies.

It is also noteworthy that, in an experiment carried out at 250 °C under the same experimental conditions and catalyst [Pd/h-ZSM-5 (122)] but adding 6 bar of nitrogen instead of hydrogen, the conversion decreased abruptly from 61 to 6%.[72] This result bears out the role of hydrogen in activating palladium sites for DC. On the basis of these results, a

https://doi.org/10.1021/acs.energyfuels.1c01373
Energy Fuels 2021, 35, 17167−17181

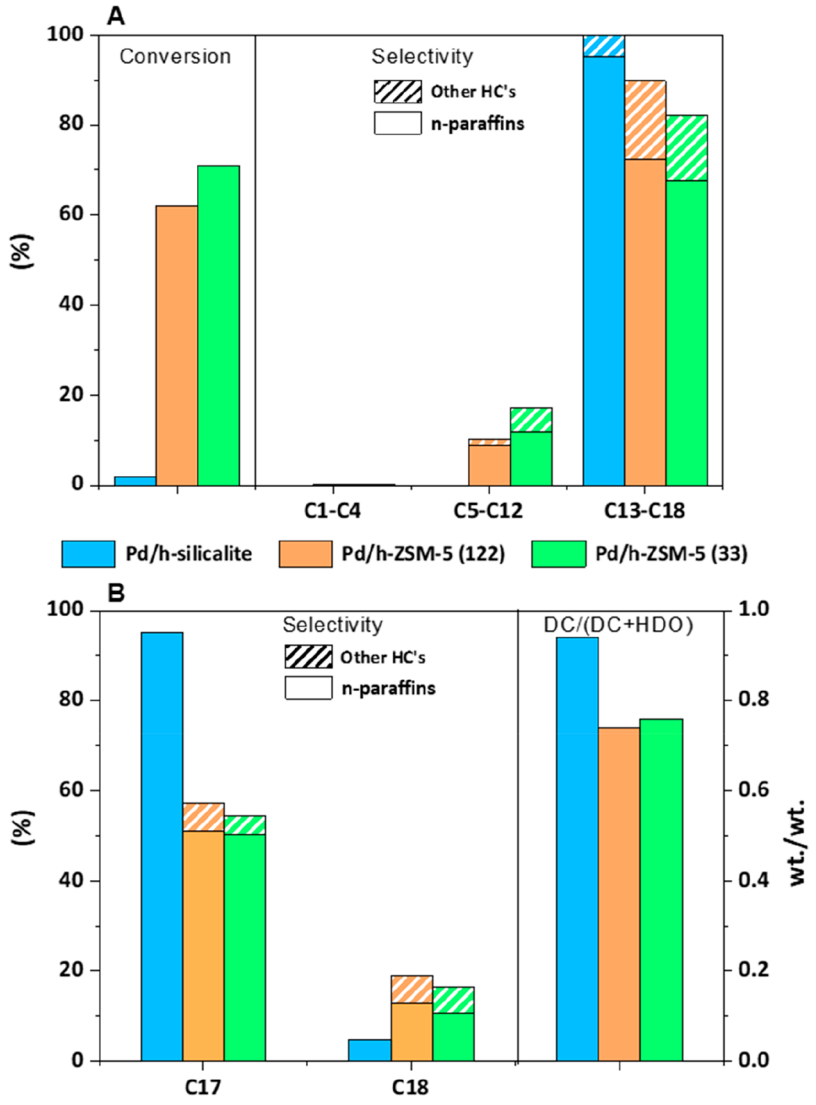

Figure 5. Influence of the Si/Al atomic ratio of the MFI support: (A) conversion and selectivity by hydrocarbon fractions along with the *n*-paraffin share and (B) selectivity toward C_{17} and C_{18} hydrocarbons and DC/(DC + HDO) ratio (T = 250 °C, t = 180 min, and P_{H_2} = 6 bar).

temperature of 250 °C was selected for further studies to limit the extension of cracking reactions and favor the stearic acid DC while still keeping a significant catalytic activity (conversion over 60%). Moreover, at this temperature, about 90% of the products correspond with diesel-range components, mainly long-chain (C_{17} and C_{18}) hydrocarbons.

3.2.3. Influence of the Hydrogen Pressure. As concluded above, the presence of hydrogen is essential to activate the Pd sites and promote the stearic acid DC. Therefore, to better establish the effect of this variable, additional experiments were carried varying the hydrogen pressure initially loaded into the reactor between 3 and 25 bar.

Figure 4A shows that the stearic acid conversion is strongly affected by the hydrogen pressure. At the lowest hydrogen pressure tested (3 bar), the conversion is relatively low (23%) and increases until reaching 89% at 25 bar. This finding confirms that the intrinsic activity of the Pd sites is sharply enhanced in the presence of hydrogen. Nevertheless, the enhancement of the conversion is more marked between 3 and 6 bar than when reaching 25 bar, indicating that a relatively low hydrogen pressure is enough to activate the Pd centers. Conversely, this variable has little effect on the product distribution per hydrocarbon fraction. Thus, independent of the hydrogen pressure, the major products of the reactions were C_{13}−C_{18} hydrocarbons (selectivity of ∼83−90%), with minor production of C_5−C_{12} compounds and negligible amounts of gaseous hydrocarbons. These results confirm the effective suppression under a H_2 atmosphere of cracking reactions, mainly of those occurring by end-chain cracking over the strong acid sites of the zeolite that would lead to C_1−C_4 hydrocarbons. With regard to the type of compounds, the products consist mostly of linear alkanes, although there is also some formation of isoparaffins, whose share tends to increase with the hydrogen pressure because it promotes the occurrence of hydroisomerization reactions.

On the other hand, as displayed in Figure 4B, the selectivities toward C_{17} and C_{18} hydrocarbons undergo significant changes with the increase of the hydrogen pressure. In this way, a lowering in the production of C_{17} components (mainly *n*-C_{17}) is observed as indicated by the drop in their selectivity from 67.5% at 3 bar to 35.3% at 25 bar. In contrast, the selectivity toward C_{18} is enhanced with the rise in hydrogen pressure, mounting from 19.6% at 3 bar to 41.2% at

https://doi.org/10.1021/acs.energyfuels.1c01373
Energy Fuels 2021, 35, 17167−17181

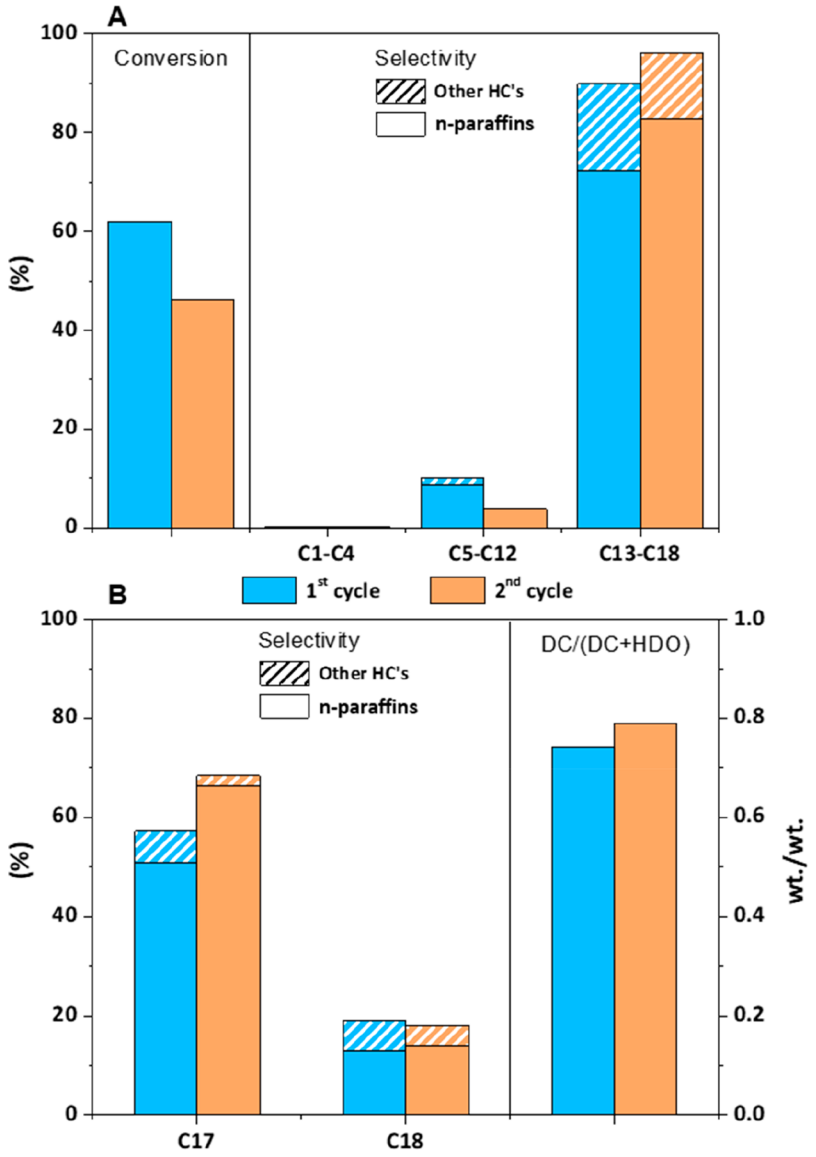

Figure 6. Reuse of the catalyst: (A) conversion and selectivity by hydrocarbon fractions along with the *n*-paraffin share and (B) selectivity toward C_{17} and C_{18} hydrocarbons and DC/(DC + HDO) ratio [T = 250 °C, t = 180 min, P_{H_2} = 6 bar, and catalyst = Pd/h-ZSM-5 (122)].

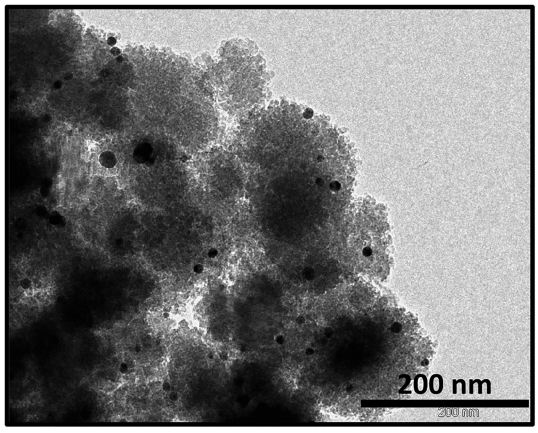

Figure 7. TEM image of the used catalyst after the first reaction cycle.

25 bar. This fact is also reflected in the DC/(DC + HDO) ratio, which decreases from 0.77 to 0.46.

Accordingly, it is concluded that the DC and HDO of stearic acid are competitive reactions, whose relative extension can be modulated by adjusting the hydrogen pressure. DC is favored at low hydrogen pressures, while the opposite occurs for HDO. This phenomenon can be explained considering that HDO proceeds with the consumption of 3 mol of hydrogen by each mole of stearic acid, whereas the stoichiometry of the DC reaction does not involve the participation of hydrogen, being only necessary for the activation of the metal phase.[78] In light of these results, a hydrogen pressure of 6 bar was selected for the following sections in the current study.

3.2.4. Effect of the Support Acidity. The acidity of the support can play an important role in the conversion of fatty acids because it may promote a variety of reactions, such as cracking and hydroisomerization. Additionally, the parent zeolite (without Pd) may exhibit itself catalytic activity for DC. To check this last possibility, the h-ZSM-5 (122) support was tested under the selected operation variables (T = 250 °C and P_{H_2} = 6 bar), resulting in a null conversion of stearic acid. This fact bears out that, when using these really mild reaction

https://doi.org/10.1021/acs.energyfuels.1c01373
Energy Fuels 2021, 35, 17167−17181

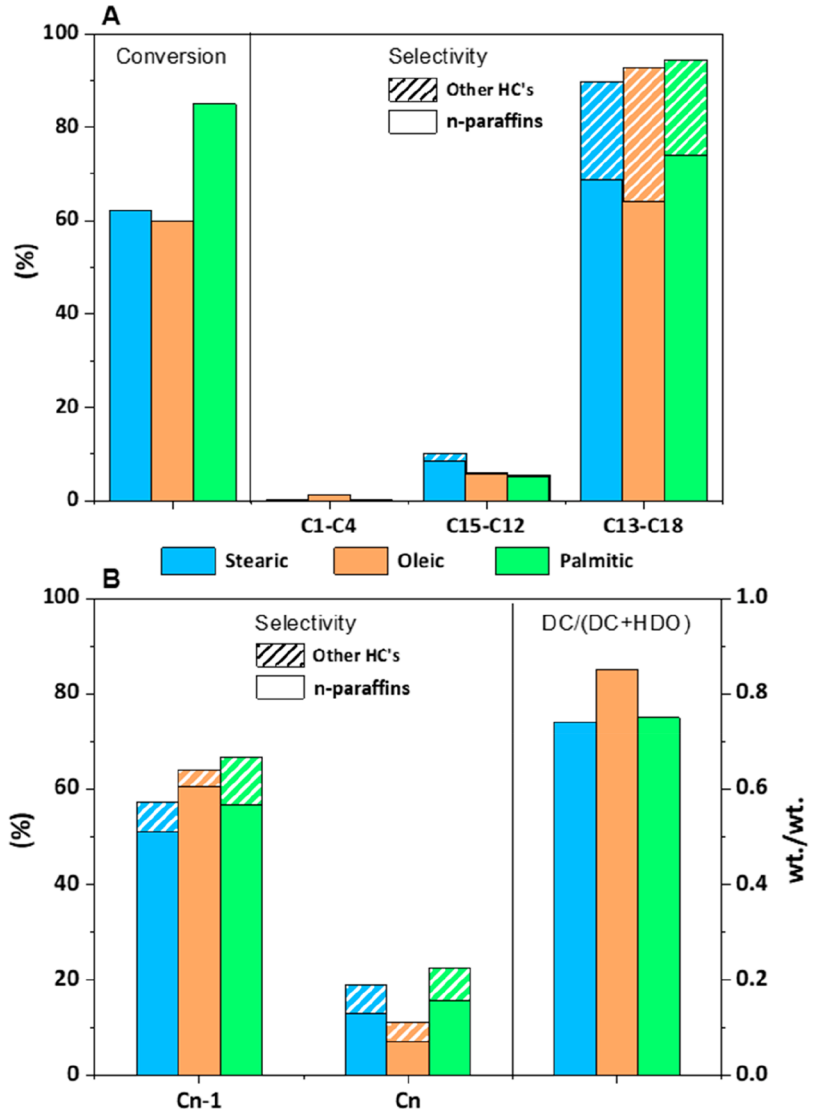

Figure 8. Influence of the fatty acid type (stearic, oleic, and palmitic acids): (A) conversion and selectivity by hydrocarbon fractions along with the *n*-paraffin share and (B) selectivity toward C_{17} and C_{18} hydrocarbons and DC/(DC + HDO) ratio [T = 250 °C, t = 180 min, P_{H_2} = 6 bar, and catalyst = Pd/h-ZSM-5 (122)].

conditions, the deoxygenation of stearic acid by both DC and HDO requires the presence of the metallic Pd centers.

Another important point to unveil is the effect of the MFI support acidity in the activation of the Pd metal sites. To that end, three catalysts having very different acid properties [Pd/h-silicalite, Pd/h-ZSM-5 (122), and Pd/h-ZSM-5 (33)] were tested. It should be notice that Pd/h-silicalite does not contains aluminum in its makeup; therefore, it lacks any mild or strong acidity.

It is clearly appreciated in Figure 5A that the conversion of stearic acid increases with the aluminum content of the catalyst, varying from a negligible 2% over Pd/h-silicalite to a remarkable 71% over Pd/h-ZSM-5 (33). Taking into account that the three catalysts show a similar Pd content (~1 wt %), it is concluded that the transformation of the fatty acid also depends heavily upon the acidity of the MFI support. Additionally, the same experiment carried out using Pd supported over a commercial ZSM-5 (Pd/n-ZSM-5), which shows a Si/Al atomic ratio of 32 and whose physicochemical properties may be found elsewhere,[72] pointed out a distinctly lower conversion (33%) than the equivalent Pd/h-ZSM-5 (33) (71%), while its selectivity toward C_{13}−C_{18} hydrocarbons was 94%, slightly higher than the 82% value attained over Pd/h-ZSM-5 (33). These results prove the advantage of using a hierarchical ZSM-5 support, because its better accessibility facilitates not only cracking but DC reactions as well, leading to a rather enhanced catalytic activity.

The small conversion obtained with Pd/h-silicalite is in contrast with previous literature that reported fatty acid DC over Pd supported on different pure silica materials, such as mesocellular foams SBA-12 and SBA-16.[59,79] This difference can be assigned to the quite lower temperature employed in the present work compared to the previous literature. The latter operate at temperatures over 300 °C, showing the need of activating the Pd nanoparticles for catalyzing the fatty acid DC over pure silica supports. Enhanced activity has been widely reported in the literature[80−83] for HDO reactions when using catalysts consisting of metals supported on acid solids. The same effect seems to apply here for the stearic acid DC. These results indicate that the ZSM-5 acid sites, although not

https://doi.org/10.1021/acs.energyfuels.1c01373
Energy Fuels 2021, 35, 17167−17181

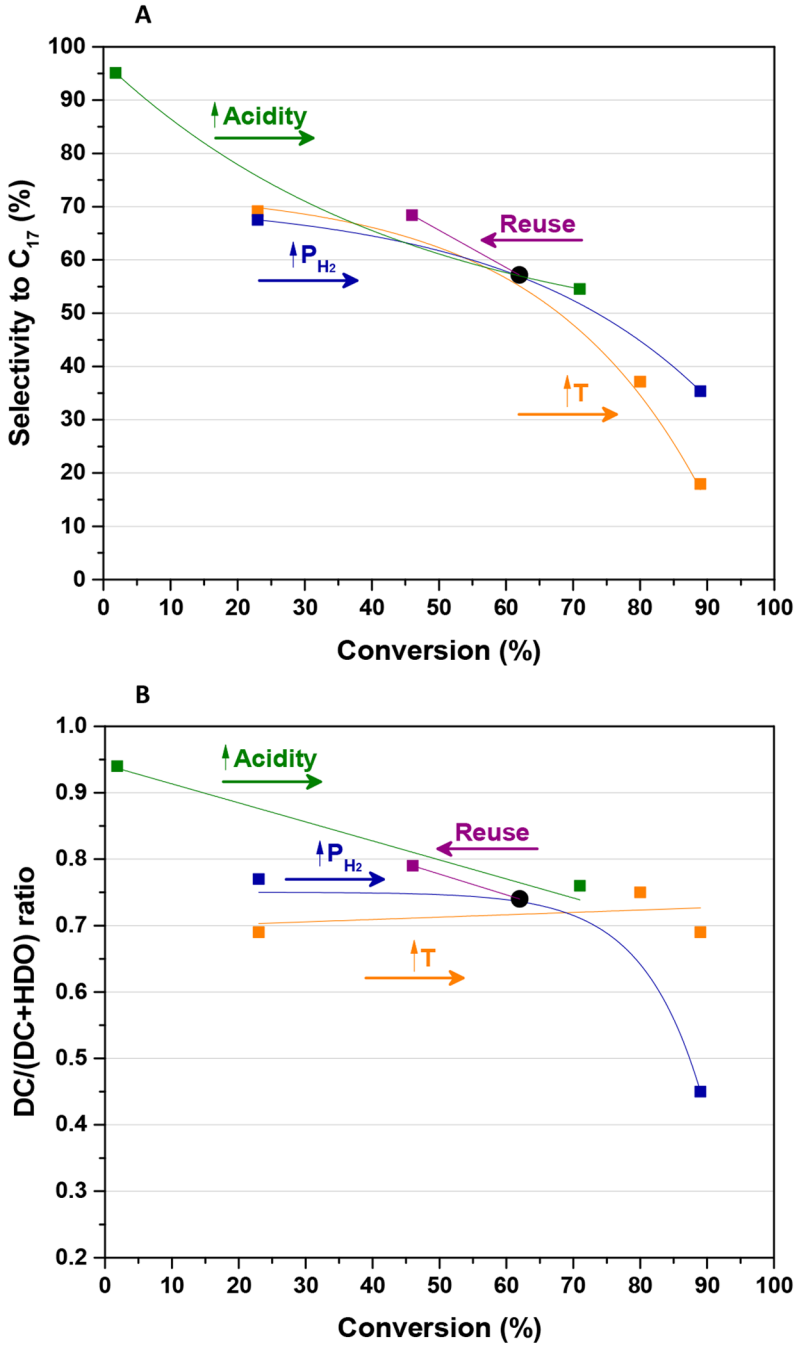

Figure 9. Relationship between (A) C_{17} selectivity or (B) DC/(DC + HDO) ratio and stearic acid conversion. The round black dot represents a common point in the temperature, pressure, acidity, and reuse series.

being directly active in the DC reaction at the temperature used here, are able to increase the intrinsic activity of the Pd sites (which, under the existing hydrogen atmosphere, are likely to be Pd−H sites). This finding can be assigned to both a better Pd dispersion when using acidic supports and the establishment of interactions between the metal and acid centers. In this regard, acidic supports have been reported to diminish the electron density over the Pd particles, leading toward a less strong adsorption of the fatty acid, which favors its DC.[60,84] Moreover, the enhanced accessibility of the Pd/h-ZSM-5 samples as a result of the presence of mesopores is expected to improve the contact between the external acid sites and the Pd metal particles, increasing their activity for stearic acid DC. On the other hand, the strong Brønsted acidity of both zeolitic supports is expected to play a key role in this interaction, because of the mobility of the proton of the Brønsted acid site, which is nearer to the Pd moiety than Al associated with the Lewis acid site, placed within the zeolite framework.

It is also noteworthy that the further increase in the stearic acid conversion observed for the catalyst with the highest Al content is relatively small. Thus, it augmented from 62% [Pd/h-ZSM-5 (122)] to just 71% [Pd/h-ZSM-5 (33)], suggesting the occurrence of an optimum Al/Pd ratio in terms of DC activity. Once this optimum ratio is reached, the presence of

https://doi.org/10.1021/acs.energyfuels.1c01373
Energy Fuels 2021, 35, 17167−17181

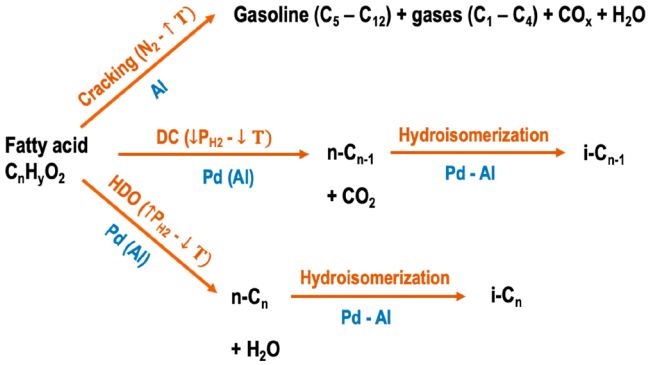

Figure 10. Reaction scheme showing the main transformation routes during the conversion of fatty acids over Pd/h-ZSM-5 catalysts.

additional acid sites does seem to significantly improve the catalytic activity of the Pd sites.

The reaction products over the ZSM-5-based catalysts are mostly $C_{13}-C_{18}$ hydrocarbons (selectivity above 80%), although their production is somewhat reduced upon increasing the acidity of the hierarchical support because cracking reactions leading toward the C_5-C_{12} fraction are promoted. Nevertheless, despite the relatively high acid site concentration in sample Pd/h-ZSM-5 (33), the selectivity toward C_1-C_4 hydrocarbons is negligible. Accordingly, even for this highly acidic support, severe cracking reactions do not take place, which can be assigned to the low reaction temperature employed.

Figure 5B shows that both ZSM-5-based catalysts present similar selectivities toward C_{17} and C_{18} hydrocarbons and, therefore, very close values of the DC/(DC + HDO) ratio. Accordingly, the variation of the support acidity does not modify the balance between both deoxygenation pathways, showing that the synergetic interactions between metallic and acid sites enhance the activity of the Pd sites in both DC and HDO reactions.

3.2.5. Catalyst Reuse. One of the possible problems associated with the catalysts used in the deoxygenation of vegetable oils, triglycerides, and fatty acids is their deactivation. There are several potential causes originating from this loss of activity, such as metal leaching, metal reoxidation, total or partial covering of the metal particles by the reactants, or adsorption of olefinic compounds[44,45] as well as coke deposition inside the pores.[85] In this regard, hierarchical zeolites show a high external/mesopore surface, which delays the clogging of the micropores by coke.[86] On the other hand, when Pd is used, the problems related to leaching and metal reoxidation are minimal,[87] whereas it has been proposed that the deactivation caused by adsorbed reactants and products over Pd supported on mesoporous silica could be removed by extraction with solvents.[79]

In the current work, to assess the extension of catalyst deactivation, a second cycle of reaction was performed with the Pd/h-ZSM-5 (122) sample. Thereby, the catalyst was recovered after reaction, washed with *n*-dodecane, and subjected to a second reaction test under the same conditions as the first cycle. As appreciated in Figure 6A, the conversion underwent a certain abatement during the second cycle of reaction (46 versus 62%), whereas some changes can be observed in the product distribution. Thus, the selectivity toward the $C_{13}-C_{18}$ fraction is increased (90 versus 96%) at the expense of a drop in the C_5-C_{12} share in the reusing test. This is accompanied by an enhancement in the proportion of linear paraffins.

On the other hand, as inferred from Figure 6B, the second cycle leads to an increase in the selectivity toward C_{17} hydrocarbons (68 versus 57%), with the same trend being observed in the selectivity toward *n*-C_{17} (66 versus 51%). Accordingly, catalyst deactivation seems to affect to a larger extent those reactions that require the participation of acid sites, such as cracking and hydroisomerization, likely as a result of the formation of carbonaceous deposits within the zeolite micropores. Additionally, the value of the DC/(DC + HDO) ratio is improved in the second reaction cycle, which denotes a larger extent of DC versus HDO. In this regard, thermogravimetric analysis (TGA) of the catalyst recovered after the first reaction cycle displayed a total weight loss of 11.2 wt %, while the corresponding one within the 250−700 °C interval was 5.2 wt %. These results suggest the occurrence of coke deposition over both the external surface/mesopores and the micropores of the Pd/h-ZSM-5 (122) catalyst. On the other hand, inductively coupled plasma (ICP) analyses of the used catalyst pointed out a Pd content similar to that of the fresh catalyst; therefore, the possibility of the occurrence of significant Pd leaching was discarded. The possibility that the loss of activity was caused by a partial oxidation of Pd was ruled out considering that the temperature of reduction of PdO was below 50 °C, according to hydrogen temperature-programmed reduction (H_2-TPR) measurements. As the reactions were carried out at 250 °C and under 6 bar of hydrogen, the occurrence of PdO_x entities was regarded as unlikely. Figure 7 illustrates the shape and size of the Pd particles of the used catalyst after the first reaction cycle. No indication of significant sintering is appreciated, with the size of the Pd particles being very similar to that corresponding to the fresh catalyst.

In summary, these results indicate that it is possible to retrieve a great deal of the original catalyst activity (74% of the conversion obtained with the fresh sample) by just washing with *n*-dodecane. Moreover, because the selectivity toward the target products is enhanced in the second cycle, just a minor decrease is observed in terms of yield. In this way, the *n*-C_{17} yield remains almost constant, with values of 31.5 and 30.6 wt % for the first and second reaction cycles, respectively.

3.2.6. Influence of the Fatty Acid Type. A number of features of the raw fatty acid, such as chain length or degree of saturation, can play an important role in its transformation via DC. Accordingly, the performance of the Pd/h-ZSM-5 (122) catalyst was compared for three different fatty acids: stearic acid [CH_3 $(CH_2)_{16}COOH$], oleic acid [$CH_3-(CH_2)_7-CH{=}CH-(CH_2)_7-COOH$], and palmitic acid [$CH_3-(CH_2)_{14}-COOH$].

Figure 8A illustrates the conversion of the fatty acid and the selectivity by the hydrocarbon fraction. The two fatty acids with 18 carbon atoms give rise to similar conversions (~60%) because their only difference lies in the presence of a double bond in the oleic acid chain, which is presumably quickly hydrogenated at the beginning of the reaction being converted into stearic acid.[44,51] With regard to the length of the fatty acid, palmitic acid shows the highest conversion (85%), with an important increase in comparison to stearic and oleic acids. This difference can be assigned to the bulkier nature of the latter, which may lead to steric or diffusional hindrances. Moreover, that enhanced polarity of palmitic acid may contribute to its adsorption and further conversion over the

https://doi.org/10.1021/acs.energyfuels.1c01373
Energy Fuels 2021, 35, 17167−17181

zeolitic support. With regard to the product distribution per fraction, just small variations can be observed, with C_{13}−C_{18} hydrocarbons remaining as the main components with selectivities over 90%.

On the other hand, as shown in Figure 8B, for the three feedstocks, the major products are the corresponding C_{n-1} hydrocarbons generated by DC with selectivities in the range of 57−67%, with the highest value being obtained with palmitic acid. The latter also leads to the largest share of nonlinear hydrocarbons for both C_{n-1} and C_n, which can be ascribed to its shorter chain length and higher polarity, which eases the accessibility and interaction with the active sites of the Pd/h-ZSM-5 (122) catalyst, wherein isomerization reactions are promoted.

Finally, the DC/(DC + HDO) ratio presents high values for the three fatty acids (over 0.74). Moreover, in the case of oleic acid, it increases significantly as a result of the partial consumption of hydrogen in the saturation of oleic acid, which may contribute to reduce the extent of the HDO pathway. These results confirm that the Pd/h-ZSM-5 catalyst is able to catalyze selectively DC reactions independently of the nature of the raw fatty acid.

3.2.7. Fatty Acid Conversion Pathways. To obtain an overall picture on how the different operation variables as well as the catalyst acidity influence the activity and product distribution, the results obtained with stearic acid have been represented in panels A and B of Figure 9 in the form of C_{17} selectivity and DC/(DC + HDC) ratio, respectively, versus the fatty acid conversion.

The relationship between C_{17} selectivity and conversion (Figure 9A) seems to follow a general decreasing trend, which is accelerated for stearic acid conversions superior to 60%. Nevertheless, this negative effect on the selectivity is somewhat more pronounced when increasing the temperature than the hydrogen pressure, which can be assigned to a higher occurrence of cracking reactions at 300 °C. In the same way, the increase of the support acidity also causes a progressive reduction in the selectivity while enhancing the conversion. However, this effect is partially reverted by the deactivation of the zeolite acidity as a result of the formation of carbon deposits, as denoted by the high selectivity obtained in the second reaction cycle. In the case of the DC/(DC + HDO) ratio (Figure 9B), it is interesting to note that this parameter remains relatively constant, with values about 0.70−0.80, independent of the stearic acid conversion. Just when working at an elevated hydrogen pressure, it decreases significantly as a result of the prevalence of HDO reactions.

On the basis of the results obtained in this work, the reaction scheme shown in Figure 10 is proposed, which includes the three major pathways for the conversion of fatty acids into liquid hydrocarbons: (a) Under an inert atmosphere (nitrogen) and temperatures above 275 °C, cracking reactions that occur over the accessible strong acid sites of hierarchical ZSM-5 prevail, leading mostly to gasoline and to a lesser extent gaseous hydrocarbons.[72] (b) DC reactions are predominant when operating at low hydrogen pressures (6 bar) and mild temperatures (225−275 °C). Under these conditions, the combination of Pd and acid sites in the catalyst leads to high conversion of the fatty acid via DC, producing C_{n-1} long-chain hydrocarbons. It is noteworthy that Pd/h-ZSM-5 shows meaningful DC activity even when operating at temperatures as low as 225 °C, in contrast with the previous literature that typically operates at 300 °C and above. (c) HDO becomes relevant for the reactions performed at relatively high hydrogen pressures (25 bar), leading to C_n long-chain hydrocarbons. This pathway is competing directly with DC because both take place with the participation of Pd sites, whose activity is enhanced by the presence of strong acidity in the support.

Finally, the primary products derived from DC and HDO reactions (linear C_{17} and C_{18} hydrocarbons, respectively) may undergo hydroisomerization reactions with the participation of both metal and acid sites, giving rise to a variety of branched paraffins.

4. CONCLUSION

Pd/h-ZSM-5 has been found to be a remarkable catalytic system for the selective DC of fatty acids as a result of the presence of a hierarchical porosity and bifunctional properties. The existence of a high share of the external/mesopore surface favors the dispersion of the Pd nanoparticles and provides enhanced accessibility, facilitating the conversion of the fatty acid molecules. The support acidity plays an essential role increasing the activity of the Pd sites as a result of both an improved metal dispersion and the establishment of interactions between metal and acid centers.

The tests performed using stearic acid as feedstock show that, although hydrogen is not required according to the stoichiometry of the DC reaction, its presence is needed to activate the Pd sites and, therefore, to produce C_{17} hydrocarbons. The best performance in terms of stearic acid conversion into C_{17} was obtained at low hydrogen pressures (6 bar), while when increasing this variable up to 25 bar, the HDO pathway is favored, leading to enhanced selectivity toward C_{18} hydrocarbons. The temperature is also an important variable because, when operating above 275 °C, cracking reactions are promoted, considerably decreasing the C_{17} selectivity. However, lowering the reaction temperature to 250 °C affords the selective formation of C_{17} hydrocarbons while keeping a high stearic acid conversion. Interestingly, the catalyst could be reused after washing with *n*-dodecane, recovering 74% of its initial activity and with just a minor loss in the C_{17} yield because deactivation preferentially affects the acid sites responsible for the non-desired cracking reactions.

Additional tests performed with oleic and palmitic acids indicate that the outstanding performance of the Pd/h-ZSM-5 catalyst is maintained independently of the fatty acid employed as feedstock. Thus, under the proper reaction conditions, this catalytic system leads to the transformation of the fatty acids with very high selectivity (over 90%) toward middle distillate hydrocarbons that contain a large share of the corresponding C_{n-1} paraffin generated by DC.

Finally, a reaction scheme is proposed accounting for the major pathways of fatty acid conversion over Pd/h-ZSM-5: DC, HDO, and cracking.

AUTHOR INFORMATION

Corresponding Author

David P. Serrano − *IMDEA Energy Institute, 28935 Móstoles, Madrid, Spain;* orcid.org/0000-0001-5383-3944; Phone: +34-91-737-11-22; Email: david.serrano@imdea.org

Authors

Marta Arroyo − *Group of Chemical and Environmental Engineering, Rey Juan Carlos University, 28933 Móstoles,*

https://doi.org/10.1021/acs.energyfuels.1c01373
Energy Fuels 2021, 35, 17167−17181

Madrid, Spain; IMDEA Energy Institute, 28935 Móstoles, Madrid, Spain

Laura Briones − *Group of Chemical and Environmental Engineering, Rey Juan Carlos University, 28933 Móstoles, Madrid, Spain;* orcid.org/0000-0001-7688-965X

Héctor Hernando − *IMDEA Energy Institute, 28935 Móstoles, Madrid, Spain*

José M. Escola − *Group of Chemical and Environmental Engineering, Rey Juan Carlos University, 28933 Móstoles, Madrid, Spain;* orcid.org/0000-0002-5342-7441

Complete contact information is available at: https://pubs.acs.org/10.1021/acs.energyfuels.1c01373

Notes

The authors declare no competing financial interest.

■ ACKNOWLEDGMENTS

The authors thank the funding received from the Spanish government through projects CTQ 2014-60209-R and CTQ2017-87001-R.

■ REFERENCES

(1) Vicente, G.; Martínez, M.; Aracil, J. Integrated biodiesel production: A comparison of different homogeneous catalysts. *Bioresour. Technol.* **2004**, *92*, 297−305.

(2) Vicente, G.; Martínez, M.; Aracil, J. Optimization of integrated biodiesel production. Part I. A study of the biodiesel purity and yield. *Bioresour. Technol.* **2007**, *98*, 1724−1733.

(3) Bautista, L. F.; Vicente, G.; Rodríguez, R.; Pacheco, M. Optimization of FAME production from waste cooking oil for biodiesel use. *Biomass Bioenergy* **2009**, *33*, 862−872.

(4) Yahya, S.; Muhamad Wahab, S. K.; Harun, F. W. Optimization of biodiesel production from waste cooking oil using Fe-Montmorillonite K10 by response surface methodology. *Renewable Energy* **2020**, *157*, 164−172.

(5) Laskar, I. B.; Deshmukhya, T.; Bhanja, P.; Paul, B.; Gupta, R.; Chatterjee, S. Transesterification of soybean oil at room temperature using biowaste as catalyst: An experimental investigation on the effect of co-solvent on biodiesel yield. *Renewable Energy* **2020**, *162*, 98−111.

(6) Roy, T.; Sahani, S.; Sharma, Y. C. Green synthesis of biodiesel from *Ricinus communis* oil (castor seed oil) using potassium promoted lanthanum oxide catalyst: Kinetic, thermodynamic and environmental studies. *Fuel* **2020**, *274*, 117644.

(7) Phromphithak, S.; Meepowpan, P.; Shimpalee, S.; Tippayawong, N. Transesterification of palm oil into biodiesel using ChOH ionic liquid in a microwave heated continuous flow reactor. *Renewable Energy* **2020**, *154*, 925−936.

(8) Guo, J.; Sun, S.; Liu, J. Conversion of waste frying palm oil into biodiesel using free lipase A from *candida antarctica* as a novel catalyst. *Fuel* **2020**, *267*, 117323.

(9) Naeem, M. M.; Al-Sakkari, E. G.; Boffito, D. C.; Gadalla, M. A.; Ashour, F. H. One-pot conversion of highly acidic waste cooking oil into biodiesel over a novel bio-based bifunctional catalyst. *Fuel* **2021**, *283*, 118914.

(10) Hájek, M.; Vávra, A.; Múck, J. Butanol as co-solvent for transesterification of rapeseed oil by methanol under homogeneous and heterogeneous catalysts. *Fuel* **2020**, *277*, 118239.

(11) Serrano, D. P.; Melero, J. A.; Morales, G.; Iglesias, J.; Pizarro, P. Progress in the design of zeolite catalysts for biomass conversion into biofuels and bio-based chemicals. *Catal. Rev.: Sci. Eng.* **2018**, *60*, 1−70.

(12) Ojeda, M.; Osterman, N.; Drazic, G.; Zilnik, L. F.; Meden, A.; Kwapinski, W.; Balu, A. M.; Likozar, B.; Tusak, N. N. Conversion of palmitic acid over bi-functional Ni/ZSM-5 catalyst: Effect of stoichiometric Ni/Al molar ratio. *Top. Catal.* **2018**, *61*, 1757−1768.

(13) Twaiq, F. A.; Zabidi, N. A. M.; Bhatia, S. Catalytic conversion of palm oil to hydrocarbons: Performance of various zeolite catalysts. *Ind. Eng. Chem. Res.* **1999**, *38*, 3230−3237.

(14) Taufiqurrahmi, N.; Mohamed, A. R.; Bhatia, S. Deactivation and coke combustion studies of nanocrystalline zeolite beta in catalytic cracking of used palm oil. *Chem. Eng. J.* **2010**, *163*, 413−421.

(15) Botas, J. A.; Serrano, D. P.; García, A.; Ramos, R. Catalytic conversion of rapeseed oil for the production of raw chemicals, fuels and carbon nanotubes over Ni-modified nanocrystalline and hierarchical ZSM-5. *Appl. Catal., B* **2014**, *145*, 205−215.

(16) Melero, J. A.; Clavero, M. M.; Calleja, G.; García, A.; Miravalles, R.; Galindo, T. Production of biofuels via the catalytic cracking of mixtures of crude vegetable oils and nonedible animal fats with vacuum gas oil. *Energy Fuels* **2010**, *24* (1), 707−717.

(17) Palankoev, T. A.; Dement'ev, K. I.; Kuznetsova, D. V.; Bondarenko, G. N.; Maximov, A. L. Acetone reaction pathway as a model bio-oxygenate in a hydrocarbon medium on zeolite Y and ZSM-5 catalyst: *In situ* FTIR study. *ACS Sustainable Chem. Eng.* **2020**, *8* (29), 10892−10899.

(18) Shimada, I.; Kato, S.; Hirazawa, N.; Nakamura, Y.; Ohta, H.; Suzuki, K.; Takatsuka, T. Deoxygenation of triglycerides by catalytic cracking with enhanced hydrogen transfer activity. *Ind. Eng. Chem. Res.* **2017**, *56*, 75−86.

(19) Xu, Z.-X.; Liu, P.; Xu, G.-S.; Liu, Q.; He, Z.-X.; Wang, Q. Biofuel oil characteristic from catalytic cracking of hydrogenated palm oil. *Energy* **2017**, *133*, 666−675.

(20) Kim, S. K.; Yoon, D.; Lee, S.-C.; Kim, J. Mo_2C/graphene nanocomposite as a hydrodeoxygenation catalyst for the production of diesel range hydrocarbons. *ACS Catal.* **2015**, *5*, 3292−3303.

(21) Wagenhofer, M. F.; Baráth, E.; Gutiérrez, O. Y.; Lercher, J. A. Carbon-carbon bond scission pathways in the deoxygenation of fatty acids on transition-metal sulfides. *ACS Catal.* **2017**, *7*, 1068−1076.

(22) Satyarthi, J. K.; Chiranjeevi, T.; Gokak, D. T.; Viswanathan, P. S. An overview of catalytic conversion of vegetable oils/fats into middle distillates. *Catal. Sci. Technol.* **2013**, *3*, 70−80.

(23) Verma, D.; Kumar, R.; Rana, B. S.; Sinha, A. K. Aviation fuel production from lipids by a single-step route using hierarchical mesoporous zeolites. *Energy Environ. Sci.* **2011**, *4*, 1667−1671.

(24) Furimsky, E. Hydroprocessing challenges in biofuels production. *Catal. Today* **2013**, *217*, 13−56.

(25) Kubička, D.; Horáček, J.; Setnička, M.; Bulánek, R.; Zukal, A.; Kubičkova, I. Effect of support-active phase interaction on the catalyst activity and selectivity in deoxygenation of triglycerides. *Appl. Catal., B* **2014**, *145*, 101−107.

(26) Yang, Y.; Ochoa-Hernández, C.; Pizarro, P.; De la Peña O'Shea, V. A.; Coronado, J. M.; Serrano, D. P. Influence of the Ni/P ratio and metal loading on the performance of Ni_xP_y/SBA-15 catalysts for the hydrodeoxygenation of methyl oleate. *Fuel* **2015**, *144*, 60−70.

(27) Yang, Y.; Ochoa-Hernández, C.; De la Peña O'Shea, V. A.; Coronado, J. M.; Serrano, D. P. Ni_2P/SBA-15 as hydrodeoxygenation catalyst with enhanced selectivity for the conversion of methyl oleate into *n*-octadecane. *ACS Catal.* **2012**, *2*, 592−598.

(28) Herreros, J. M.; Jones, A.; Sukjit, E.; Tsolakis, A. Blending lignin-derived oxygenate in enhanced multi-component diesel fuel for improved emissions. *Appl. Energy* **2014**, *116*, 58−65.

(29) Moore, R. H.; Thornhill, K. L.; Weinzierl, B.; Sauer, D.; D'Ascoli, E.; Kim, J.; Lichtenstern, M.; Scheibe, M.; Beaton, B.; Beyersdorf, A. J.; Barrick, J.; Bulzan, D.; Corr, C. A.; Crosbie, E.; Jurkat, T.; Martin, R.; Riddick, D.; Shook, M.; Slover, G.; Voigt, C.; White, R.; Winstead, E.; Yasky, R.; Ziemba, L. D.; Brown, A.; Schlager, H.; Anderson, B. E. Biofuel blending reduces particle emissions from aircraft engines at cruise conditions. *Nature* **2017**, *543*, 411−415.

(30) Coumans, A. E.; Hensen, E. J. M. A model compound (methyl oleate, oleic acid, triolein) study of triglycerides hydrodeoxygenation over alumina-supported NiMo sulfide. *Appl. Catal., B* **2017**, *201*, 290−301.

(31) Ameen, M.; Azizan, M. T.; Yusup, S.; Ramli, A.; Shahbaz, M.; Aqsha, A.; Kaur, K.; Wai, C. K. Parametric studies on hydro-

deoxygenation of rubber seed oil for diesel range hydrocarbon production. *Energy Fuels* **2020**, *34*, 4603−4617.
(32) Janampelli, S.; Darbha, S. Metal oxide-promoted hydrodeoxygenation activity of platinum in Pt-MO_x/Al_2O_3 catalysts for green diesel production. *Energy Fuels* **2018**, *32*, 12630−12643.
(33) Kukushkin, R. G.; Yeletsky, P. M.; Grassin, C. T.; Chen, B.-H.; Bulavchenko, O. A.; Saraev, A. A.; Yakovlev, V. A. Deoxygenation of esters over sulfur-free Ni-W/Al_2O_3 catalysts for production of biofuel components. *Chem. Eng. J.* **2020**, *396*, 125202.
(34) Yoosuk, B.; Sanggam, P.; Wiengket, S.; Prasassarakich, P. Hydrodeoxygenation of oleic acid and palmitic acid to hydrocarbon-like biofuel over unsupported Ni-Mo and Co-Mo sulfide catalysts. *Renewable Energy* **2019**, *139*, 1391−1399.
(35) Hocevar, B.; Grilc, M.; Hus, M.; Likozar, B. Mechanism, ab initio calculations and microkinetics of straight-chain alcohol, ether, ester, aldehyde and carboxylic acid hydrodeoxygenation over Ni-Mo catalyst. *Chem. Eng. J.* **2019**, *359*, 1339−1351.
(36) Neste. *NEXBTL Technology*; https://www.neste.com/about-neste/innovation/nexbtl-technology.
(37) Eni. https://www.eni.com/en-IT/operations/biorefineries.html.
(38) Preem. https://www.preem.com/in-english/press/.
(39) UPM. https://www.upm.com/businesses/upm-biofuels/.
(40) Zhang, H.; Lin, H.; Zheng, Y. The role of cobalt and nickel in deoxygenation of vegetable oils. *Appl. Catal., B* **2014**, *160−161*, 415−422.
(41) Horacek, J.; Tisler, Z.; Rubas, V.; Kubička, D. HDO catalysts for triglycerides conversion into pyrolysis and isomerization feedstock. *Fuel* **2014**, *121*, 57−64.
(42) Santillan-Jimenez, E.; Crocker, M. Catalytic deoxygenation of fatty acids and their derivatives to hydrocarbon fuels via decarboxylation/decarbonylation. *J. Chem. Technol. Biotechnol.* **2012**, *87*, 1041−1050.
(43) Simakova, I.; Simakova, O.; Mäki-Arvela, P.; Murzin, D. Y. Decarboxylation of fatty acids over Pd supported on mesoporous carbon. *Catal. Today* **2010**, *150*, 28−31.
(44) Immer, J. G.; Kelly, M. J.; Lamb, H. H. Catalytic reaction pathways in liquid-free deoxygenation of C18 free fatty acids. *Appl. Catal., A* **2010**, *375*, 134−139.
(45) Ping, E. W.; Wallace, R.; Pierson, J.; Fuller, T. F.; Jones, C. W. Highly dispersed palladium nanoparticles on ultra-porous silica mesocellular foam for the catalytic decarboxylation of stearic acid. *Microporous Mesoporous Mater.* **2010**, *132*, 174−180.
(46) Wu, J.; Shi, J.; Fu, J.; Leidl, J. A.; Hou, Z.; Lu, X. Catalytic decarboxylation of fatty acids to aviation fuels over nickel supported on activated carbon. *Sci. Rep.* **2016**, *6*, 27820.
(47) Fu, J.; Lu, X.; Savage, P. E. Hydrothermal decarboxylation and hydrodeoxygenation of fatty acids over Pt/C. *ChemSusChem* **2011**, *4*, 481−486.
(48) Madsen, A. T.; Rozmyslowicz, B.; Simakova, I. L.; Kilpio, T.; Leino, A.-R.; Kordás, K.; Eränen, K.; Mäki-Arvela, P.; Murzin, D. Y. Step changes and deactivation behaviour in the continuous decarboxylation of stearic acid. *Ind. Eng. Chem. Res.* **2011**, *50*, 11049−11058.
(49) Shim, J. O.; Jeong, D.-W.; Jang, W.-J.; Jeon, K.-W.; Kim, S.-H.; Jeon, B.-H.; Roh, H.-S.; Na, J.-G.; Oh, Y.-K.; Han, S. S.; Ko, C. H. Optimization of unsupported CoMo catalysts for decarboxylation of oleic acid. *Catal. Commun.* **2015**, *67*, 16−20.
(50) Snåre, M.; Kubičková, I.; Mäki-Arvela, P.; Eränen, K.; Murzin, D. Y. Heterogeneous catalytic deoxygenation of stearic acid for production of biodiesel. *Ind. Eng. Chem. Res.* **2006**, *45*, 5708−5715.
(51) Immer, J. G.; Lamb, H. H. Fed-batch catalytic deoxygenation of free fatty acids. *Energy Fuels* **2010**, *24*, 5291−5299.
(52) Ford, J. P.; Immer, J. G.; Lamb, H. H. Palladium catalysts for fatty acid deoxygenation: Influence of the support and fatty acid chain length on decarboxylation kinetics. *Top. Catal.* **2012**, *55*, 175−184.
(53) Hossain, M. Z.; Chowdhury, M. B. I.; Jhawar, A. K.; Xu, W. Z.; Biesinger, M. C.; Charpentier, P. A. Continuous hydrothermal decarboxylation of fatty acids and their derivatives into liquid hydrocarbons using Mo/Al_2O_3. *ACS Omega* **2018**, *3* (6), 7046−7060.
(54) Grilc, M.; Likozar, B. Levulinic acid hydrodeoxygenation, decarboxylation and oligomerization over NiMo/Al2O3 catalyst to bio-based value-added chemicals: Modelling of mass transfer, thermodynamics and microkinetics. *Chem. Eng. J.* **2017**, *330*, 383−397.
(55) Loe, R.; Lavoignat, Y.; Maier, M.; Abdallah, M.; Morgan, T.; Qian, D.; Pace, R.; Santillan-Jimenez, E.; Crocker, M. Continuous catalytic deoxygenation of waste free fatty acid-based feeds to fuel-like hydrocarbons over a supported Ni-Cu catalyst. *Catalysts* **2019**, *9*, 123.
(56) Liu, Y.; Yang, X.; Liu, H.; Ye, X.; Wei, Z. Nitrogen-doped mesoporous carbon supported Pt nanoparticles as a highly efficient catalyst for decarboxylation of saturated and unsaturated fatty acid to alkanes. *Appl. Catal., B* **2017**, *218*, 679−689.
(57) Jiraroj, D.; Jirarattanapochai, O.; Anutrasakda, W.; Samec, J. S. M.; Tungasmita, D. N. Selective decarboxylation of bio-based fatty acids using a Ni-FSM-16 catalyst. *Appl. Catal., B* **2021**, *291*, 120050.
(58) Foraita, S.; Liu, Y.; Haller, G. L.; Baráth, E.; Zhao, C.; Lercher, J. A. Controlling hydrodeoxygenation of stearic acid to *n*-heptadecane and *n*-octadecane by adjusting the chemical properties of Ni/SiO_2-ZrO_2. *ChemCatChem* **2017**, *9* (1), 195−203.
(59) Raut, R.; Banakar, V. V.; Darbha, S. Catalytic decarboxylation of non-edible oils over three-dimensional, mesoporous silica supported Pd. *J. Mol. Catal. A: Chem.* **2016**, *417*, 126−134.
(60) Serrano, D. P.; Escola, J. M.; Briones, L.; Arroyo, M. Selective hydrodecarboxylation of fatty acids into long-chain hydrocarbons catalyzed by Pd/Al-SBA-15. *Microporous Mesoporous Mater.* **2019**, *280*, 88−96.
(61) Al Alwan, B.; Salley, S. O.; Ng, K. Y. S. Biofuels production from hydrothermal decarboxylation of oleic acid and soybean oil over Ni-based transition metal carbides supported on Al-SBA-15. *Appl. Catal., A* **2015**, *498*, 32−40.
(62) Yang, L.; Ruess, G. L.; Carreon, M. A. Cu, Al and Ga based metal organic framework catalysts for the decarboxylation of oleic acid. *Catal. Sci. Technol.* **2015**, *5* (5), 2777−2782.
(63) Yang, L.; Tate, K. L.; Jasinski, J. B.; Carreon, M. A. Decarboxylation of oleic acid to heptadecane over Pt supported on a zeolite 5A beads. *ACS Catal.* **2015**, *5*, 6497−6502.
(64) Ahmadi, M.; Nambo, A.; Jasinski, J. B.; Ratnasamy, P.; Carreon, M. A. Decarboxylation of oleic acid over Pt catalysts supported on small-pore zeolites and hydrotalcite. *Catal. Sci. Technol.* **2015**, *5*, 380−388.
(65) Gómez, J. M.; Díez, E.; Rodríguez, A.; Palanca, R. Thermocatalytic deoxygenation of methyl laurate over potassium FAU zeolites. *Microporous Mesoporous Mater.* **2019**, *284*, 122−127.
(66) Crawford, J. M.; Zaccarine, S. F.; Kovach, N. C.; Smoljan, C. S.; Lucero, J.; Trewyn, B. G.; Pylypenko, S.; Carreon, M. A. Decarboxylation of stearic acid over Ni/MOR catalysts. *J. Chem. Technol. Biotechnol.* **2020**, *95*, 102−110.
(67) Crawford, J. M.; Smoljan, C. S.; Lucero, J.; Carreon, M. A. Deoxygenation of stearic acid over Cobalt-based NaX zeolite catalysts. *Catalysts* **2019**, *9*, 42.
(68) Serrano, D. P.; Aguado, J.; Escola, J. M.; Rodriguez, J. M.; Peral, A. Hierarchical zeolites with enhanced textural and catalytic properties synthesized from organofunctionalized seeds. *Chem. Mater.* **2006**, *18*, 2462−2464.
(69) Emeis, C. A. Determination of integrated molar extinction coefficients for infrared absorption bands of pyridine absorbed on a solid acid catalyst. *J. Catal.* **1993**, *141*, 347−354.
(70) Serrano, D. P.; Escola, J. M.; Briones, L.; Arroyo, M. Hydroprocessing of the LDPE thermal cracking oil into transportation fuels over Pd supported on hierarchical ZSM-5 catalyst. *Fuel* **2017**, *206*, 190−198.
(71) Hunns, J. A.; Arroyo, M.; Lee, A. F.; Escola, J. M.; Serrano, D.; Wilson, K. Hierarchical mesoporous Pd/ZSM-5 for the selective catalytic hydrodeoxygenation of m-cresol to methylcyclohexane. *Catal. Sci. Technol.* **2016**, *6*, 2560−2564.

https://doi.org/10.1021/acs.energyfuels.1c01373
Energy Fuels 2021, 35, 17167−17181

(72) Arroyo, M.; Briones, L.; Escola, J. M.; Serrano, D. P. Conversion of stearic acid into bio-gasoline over Pd/ZSM-5 catalysts with enhanced accessibility. *Appl. Sci.* **2019**, *9* (11), 2386.
(73) Serrano, D. P.; Aguado, J.; Escola, J. M.; Rodríguez, J. M. Nanocrystalline ZSM-5: A highly active catalyst for polyolefin feedstock recyling. *Stud. Surf. Sci. Catal.* **2002**, *142*, 77−84.
(74) Ishihara, A.; Tsuchimori, Y.; Hashimoto, T. Dehydrogenation-cracking of methyl oleate by Pt catalysts supported on a ZSM-5-Al_2O_3 hierarchical composite. *RSC Adv.* **2021**, *11*, 19864−19873.
(75) Ishihara, A.; Kanamori, S.; Hashimoto, T. Effect of Zn addition into ZSM-5 zeolite on dehydrocyclization-cracking of soybean oil using hierarchical zeolite-Al_2O_3 composite-supported Pt/NiMo sulfided catalysts. *ACS Omega* **2021**, *6*, 5509−5517.
(76) Ishihara, A.; Ishida, R.; Ogiyama, T.; Nasu, H.; Hashimoto, T. Dehydrociclization-cracking reaction of soybean oil using zeolite-metal oxide composite-supported PtNiMo sulfided catalyst. *Fuel Process. Technol.* **2017**, *161*, 17−22.
(77) Berenblyum, A. S.; Danyushevsky, V. Ya.; Katsman, E. A.; Podoplelova, T. A.; Flid, V. R. Production of engine fuels from inedible vegetable oils and fats. *Pet. Chem.* **2010**, *50*, 305−311.
(78) Sotelo-Boyas, R.; Liu, Y.; Minowa, T. Renewable diesel production for the hydrotreating of rapeseed oil with Pt/zeolite and NiMo/Al_2O_3 catalysts. *Ind. Eng. Chem. Res.* **2011**, *50*, 2791−2799.
(79) Ping, E. W.; Pierson, J.; Wallace, R.; Miller, J. T.; Fuller, T. F.; Jones, C. W. On the nature of the deactivation of supported palladium nanoparticle catalysts in the decarboxylation of fatty acids. *Appl. Catal., A* **2011**, *396*, 85−90.
(80) Janampelli, S.; Sethia, G.; Darbha, S. Selective bifunctional Cu-WO_x catalyst for hydrodeoxygenation of fatty acids. *Catal. Sci. Technol.* **2020**, *10* (1), 268−277.
(81) Sankaranarayanan, T. M.; Kreider, M.; Berenguer, A.; Gutiérrez-Rubio, S.; Moreno, I.; Pizarro, P.; Coronado, J. M.; Serrano, D. P. Cross reactivity of guaicol and propionic acid blends during hydrodeoxygenation over Ni-supported catalysts. *Fuel* **2018**, *214*, 187−195.
(82) Schreiber, M. W.; Rodríguez-Niño, D.; Gutiérrez, O. Y.; Lercher, J. A. Hydrodeoxygenation of fatty acid esters catalyzed by Ni on nano-sized MFI type zeolites. *Catal. Sci. Technol.* **2016**, *6* (22), 7976−7989.
(83) Kumar, P.; Yenumala, S. R.; Maity, S. K.; Shee, D. Kinetics of hydrodeoxygenation of stearic acid using supported nickel catalysts: Effect of supports. *Appl. Catal., A* **2014**, *471*, 28−38.
(84) Stakheev, A. Y.; Zhang, Y.; Ivanov, A. V.; Baeva, G. N.; Ramaker, D. E.; Koningsberger, D. C. Separation of geometric and electronic effects of the support on the CO and H_2 chemisorption properties of supported Pt particles: The effect of ionicity in modified alumina supports. *J. Phys. Chem. C* **2007**, *111*, 3938−3948.
(85) Lestari, S.; Maki-Arvela, P.; Bernas, H.; Simakova, O.; Sjoholm, R.; Beltramini, J.; Lu, G. Q. M.; Myllyoja, J.; Simakova, I.; Murzin, D. Y. Catalytic deoxygenation of stearic acid in a continuous reactor over mesoporous carbon-supported Pd catalyst. *Energy Fuels* **2009**, *23*, 3842−3845.
(86) Srivastava, R.; Choi, M.; Ryoo, R. Mesoporous materials with zeolite framework: Remarkable effect of the hierarchical structure for retardation of catalyst deactivation. *Chem. Commun.* **2006**, *43*, 4489−4491.
(87) Kikhtyanin, O. V.; Rubanov, A. E.; Ayupov, A. B.; Echevsky, G. V. Hydroconversion of sunflower oil on Pd/SAPO-31 catalyst. *Fuel* **2010**, *89*, 3085−3092.

https://doi.org/10.1021/acs.energyfuels.1c01373
Energy Fuels 2021, 35, 17167−17181